Calibrating photometric redshifts with intensity mapping observations

All of us[1]
[1]*University of Wherever*
(Dated: January 11, 2017)

TODO: Lorem ipsum dolor sit amet, consectetuer adipiscing elit. Ut purus elit, vestibulum ut, placerat ac, adipiscing vitae, felis. Curabitur dictum gravida mauris. Nam arcu libero, nonummy eget, consectetuer id, vulputate a, magna. Donec vehicula augue eu neque. Pellentesque habitant morbi tristique senectus et netus et malesuada fames ac turpis egestas. Mauris ut leo. Cras viverra metus rhoncus sem. Nulla et lectus vestibulum urna fringilla ultrices. Phasellus eu tellus sit amet tortor gravida placerat. Integer sapien est, iaculis in, pretium quis, viverra ac, nunc. Praesent eget sem vel leo ultrices bibendum. Aenean faucibus. Morbi dolor nulla, malesuada eu, pulvinar at, mollis ac, nulla. Curabitur auctor semper nulla. Donec varius orci eget risus. Duis nibh mi, congue eu, accumsan eleifend, sagittis quis, diam. Duis eget orci sit amet orci dignissim rutrum.

I. INTRODUCTION

TODO: Nam dui ligula, fringilla a, euismod sodales, sollicitudin vel, wisi. Morbi auctor lorem non justo. Nam lacus libero, pretium at, lobortis vitae, ultricies et, tellus. Donec aliquet, tortor sed accumsan bibendum, erat ligula aliquet magna, vitae ornare odio metus a mi. Morbi ac orci et nisl hendrerit mollis. Suspendisse ut massa. Cras nec ante. Pellentesque a nulla. Cum sociis natoque penatibus et magnis dis parturient montes, nascetur ridiculus mus. Aliquam tincidunt urna. Nulla ullamcorper vestibulum turpis. Pellentesque cursus luctus mauris.

II. FORMALISM

A. Clustering-based photo-z calibration

Consider two galaxy samples with redshift distributions $\phi_i(z)$ ($i = \{1,2\}$), and let $a^i_{\ell m}$ be the harmonic coefficients of their projected overdensity of counts on the sky. Their cross-correlation is given by:

$$\langle a^i_{\ell m}(a^j_{\ell m})^* \rangle = N^{ij}_\ell + S^{ij}_\ell \tag{1}$$

$$S^{ij}_\ell = \frac{2}{\pi} \int dz \int dz' \, \phi_i(z)\phi_j(z') \times \tag{2}$$

$$\times \int dk \, k^2 \, b_i(z)b_j(z')P_m(k,z,z') \, j_\ell(k\chi(z)) \, j_\ell(k\chi(z')),$$

where P_m is the matter power spectrum, $j_\ell(x)$ is a spherical Bessel function, N^{ij}_ℓ is the cross-noise power spectrum between samples i and j, b_i is the linear bias of the i-th sample and we have neglected redshift-space distortions and all other sub-dominant contributions to the observed power spectrum. In the Limber approximation ($j_\ell(x) \to \sqrt{\pi/(2\ell+1)}\delta^{\mathcal{D}}(\ell+1/2-x)$), this simplifies to:

$$S^{ij}_\ell = \int dk \, P_m(k,z_\ell) \frac{H^2(z_\ell)b^i(z_\ell)b^j(z_\ell)}{\ell + 1/2}\phi_i(z_\ell)\phi_j(z_\ell), \tag{3}$$

where $\chi(z_\ell) \equiv (\ell + 1/2)/k$.

For the purposes of this discussion, the most important feature of Equation 3 is the fact that the amplitude of the cross-correlation is proportional to the overlap between the redshift distributions of those samples. This is especially relevant if one of the samples has good radial resolution, in which case it can be split into narrow bins of redshift. The cross-correlations of all narrow bins with the other sample will therefore trace the amplitude of its redshift distribution, and can effectively be used to constrain it. This is illustrated in Fig. 1, which shows the cross-power spectrum between a Gaussian photo-z bin of width $\sigma = 0.05$ and a set of narrow redshift bins ($\delta z \sim 0.002$).

Different recipes have been formulated to carry out this kind of analysis, such as the optimal quadratic estimator method of [**?**]. The forecasts presented here will interpret the redshift distribution (in a parametric or non-parametric form) as a set of extra nuisance parameters, on which we will carry out the Fisher matrix analysis described in Section II D. Thus, even though our results will be optimistic in as much as the Fisher matrix saturates the Rao-Cramer bound, they will account for all correlations between redshift distribution parameters and with the cosmological parameters, as well as the presence of redshift-space distortions and magnification bias (effects that have been overseen in previous works).

For the purposes of estimating the ability of future surveys to calibrate photometric redshift distributions through cross-correlations, we will always consider an individual redshift bin for a photometric sample with unknown distribution together with a set of overlapping narrow redshift bins of spectroscopic galaxies or intensity mapping observations. Let $N^p(z)$ be the overall true redshift distribution of the photometric sample, and let $p(z_{\rm ph}|z)$ be the conditional distribution for a photo-z $z_{\rm ph}$ given the true redshift z. Then, the redshift distribution in a photo-z redshift bin b with bounds $z^i_b < z_{\rm ph} < z^f_b$ is given by

$$\phi_b(z) \propto N^p(z) \int_{z^i_b}^{z^f_b} dz_{\rm ph} \, p(z_{\rm ph}|z). \tag{4}$$

In what follows we will consider 3 degrees of complexity in terms of describing the unknown redshift distribution:

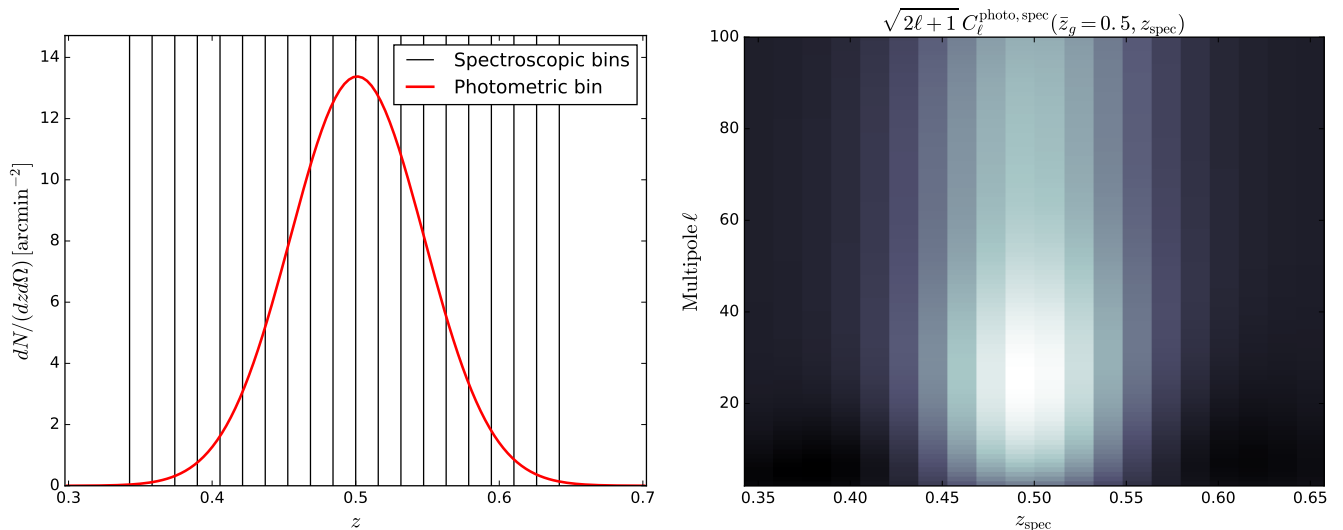1. We will assume Gaussianly-distributed photo-zs

FIG. 1: *Left panel:* example of a redshift bin for a photometric survey and the redshift bins chosen for an overlapping spectroscopic survey. *Right panel:* amplitude of the cross-correlation with an overlapping spectroscopic survey as a function of spectroscopic redshift bin (x axis) and angular scale (y axis). The amplitude of the cross-correlation traces the redshift distribution, and can therefore be used to constrain it.

with a given variance (σ_z^2) and bias Δz:

$$p(z_{\rm ph}|z) \equiv \mathcal{N}(z_{\rm ph} - \Delta z; z, \sigma_z)$$

$$\equiv \frac{\exp\left[-\frac{1}{2}\frac{(z_{\rm ph}-z-\Delta z)^2}{\sigma_z^2}\right]}{\sqrt{2\pi}\sigma_z}, \qquad (5)$$

and we will assume that the uncertainty in the redshift distribution is fully described by Δz and σ_z.

2. We will introduce hard tails in the photo-z distribution (possibly caused by catastrophic outliers) and parametrize it by a Voigt profile, combining a Gaussian and Cauchy distributions. The tails are thus parametrized by γ_L, the half-width at half-maximum of the Cauchy component. The exact form of the Voigt profile used here is described in Appendix D.

3. We will use a non-parametric form for $\phi_b(z)$, given as a piecewise function with a free amplitude for each spectroscopic redshift bin.

Our assumed fiducial value for Δz, σ_z and γ, as well as the binning scheme used are described in Section II B.

We finish this section by noting that the use of cross-correlations with spectroscopic surveys or intensity mapping observations for photo-z calibration is not limited to the measurement of the redshift distribution of a given galaxy sample, but that they can also be used to improve the precision of photometric redshift estimates for individual galaxies (e.g. [?]). Although we leave the discussion of this possibility for future work, we describe a Bayesian formalism for this task in Appendix A.
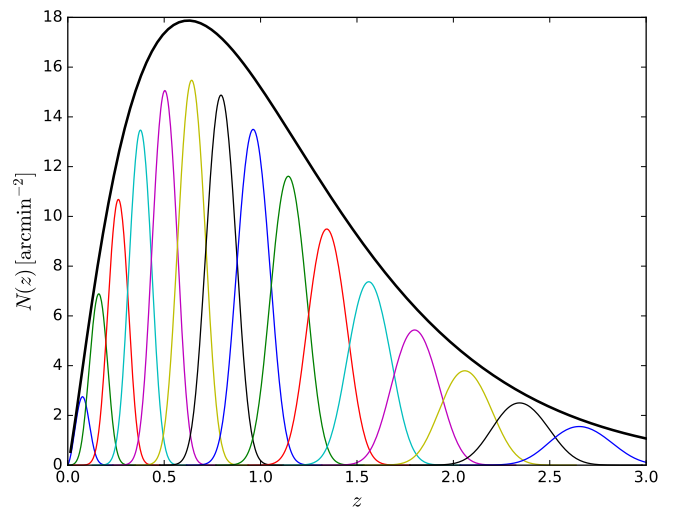

FIG. 2: Angular number density of galaxies as a function of redshift for the LSST gold sample (solid black line). The colored lines in show the window functions of the 15 redshift bins considered here.

B. Photometric redshift surveys

This section describes the model used here for a LSST-like photometric redshift survey. As in [?], we base our description of the number density of sources and their magnification bias on the measurements of the luminosity function of [?], with k-corrections computed with `kcorrect` [?]. We assume a magnitude cut of 25.3 in the i band, corresponding to the so-called "gold" sample [?]. Unlike [?], and for simplicity, we will consider a

Experiment	SKA	HIRAX
T_{inst}	25K	50 K
t_{tot}	10^4 h	2.8×10^4 h
N_{dish}	197	1024 (32×32)
D_{dish}	15 m	5 m
freq. range	350-1050 MHz	400-800 MHz
f_{sky}	0.4	0.4

TABLE I: Experimental specifications assumed for SKA and HIRAX.

single galaxy population, instead of splitting it into "red" and "blue" sources. The resulting redshift distribution is shown by the solid black line in Figure 2.

We model the linear galaxy bias as a function of redshift as $b(z) = 1 + 0.84z$, based on the simulations of [?], and quoted in the LSST science book [?].

The photometric redshift requirement for the gold sample as stated in the LSST science book are $\sigma_z/(1 + z) < 0.05$, with a goal of 0.02. Here we have taken a conservative estimate, assuming a standard deviation $\sigma_z = 0.03(1 + z)$. We then split the full sample into redshift bins with a width given by $3 \times \hat{\sigma}_z$, where $\hat{\sigma}_z$ is the photo-z variance at the bin centre. This binning scheme is chosen to reduce the correlation between bins induced by the tails of the photo-z distribution, and results in the 15 redshift bins shown in Fig. 2 (where the redshift distributions are computed with Eq. 4. Our fiducial photo-z model will assume unbiased Gaussian distributions, fully determined by σ_z. When considering biased and hard-tailed distributions parametrized as Voigt profiles we will assume $\Delta z = 0$ and $\gamma_L = 0$ for our fiducial model.

C. Intensity mapping

Intensity mapping (IM) is a novel observational technique that tries to circumvent the long integration times needed to obtain reliable spectroscopic redshifts for individual objects through an approach that is transverse to that used by photometric surveys. The idea **TODO: cites** is to observe the unresolved combined emission of many line-emitting sources in a relatively wide pixel at different frequencies. The signal-to-noise ratio of the corresponding line emission is much stronger than that of the individual sources, and thus, combining the intensity measured across the sky and relating the intensity observed at a given frequency to the rest-frame wavelength of the emission line it is possible to produce three-dimensional maps of the density of the line-emitting species. This technique is particularly appealing for isolated spectral lines, as is the case of the 21cm line caused by the spin-flip transition in neutral Hydrogen atoms (HI), and thus HI intensity mapping has been proposed as an ideal method to cover vast volumes at relatively low cost.

A number of experiments have been proposed to carry out IM measurements of the baryon acoustic oscillation scale, such as **TODO: add experiments with references**. The different instrumental approaches to IM can be broadly classified into two camps:

- *Interferometers:* the sky emission is measured by a set of antennas, and the measurements of pairs of antennas separated by a given baseline **d** are cross-correlated to produce the measurement of an angular Fourier mode with scale $\mathbf{l} \sim 2\pi\mathbf{d}/\lambda$ (where λ is the observed wavelength). The intensity map is then reconstructed by combining pairs with different baselines.

- *Single-dish:* in this case the sky emission is measured and auto-correlated by individual antennas. A band-limited intensity map with a resolution $\delta\theta \sim \lambda/D_{\text{dish}}$ is then produced by varying the antenna pointing, where D_{dish} is the antenna diameter.

The expressions for the noise power spectrum for both cases are derived in Appendix C, and can be summarized as:

$$N_{\mathbf{l}}^{\nu} = \frac{T_{\text{sys}}^2 4\pi f_{\text{sky}}}{\eta^2 \Delta\nu t_{\text{tot}}} \begin{cases} \frac{1}{N_{\text{dish}} B^2(\mathbf{l})}, & \text{single dish} \\ \frac{\Omega_p}{N_d(\mathbf{d}=\mathbf{l}\lambda/(2\pi))\lambda^2}, & \text{interferometer.} \end{cases}$$
(6)

Here T_{sys} is the system temperature, given as a combination of instrumental and sky temperature (see Appendix C), f_{sky} is the sky fraction covered by the observations, η^2 is the antenna efficiency[1], $\Delta\nu$ is the band width in that channel, t_{tot} is the total observation time for the survey, N_{dish} is the number of dishes, $B(\mathbf{l})$ is the harmonic transform of the antenna beam, $N_d(\mathbf{d})$ is the distribution of baselines and Ω_p is the solid angle covered per pointing. For all experiments discussed here we will assume $\eta = 1$, Gaussian beams so that $B(\mathbf{l}) = \exp[-l(l+1)\theta_{\text{FWHM}}^2/(16 \log 2)]$, and $\Omega_p = \theta_{\text{FWHM}}^2$, where θ_{FWHM} is the beam full-width at half maximum, which will approximate as $\theta_{\text{FWHM}} = 1.22\lambda/D_{\text{dish}}$. Note that the baseline distribution N_d is normalized such that:

$$\frac{N_{\text{dish}}(N_{\text{dish}} - 1)}{2} = \int d\mathbf{d}^2 \, N_d(\mathbf{d}),$$
(7)

where $N_{\text{dish}}(N_{\text{dish}} - 1)/2$ is the total number of independent baselines.

TODO: Introduce and describe SKA and HIRAX. See specifications in Table I.

Besides SKA and HIRAX we will also explore the capabilities of generic single-dish and interferometer experiments in terms of photo-z calibration. We will parametrize these in terms of their instrument temperature T_{inst} and the minimum or maximum angular scale that they are able to probe. On the one hand, single-dish experiments are limited on small angular scales by the beam size, which is governed by the dish diameter D_{dish}. On the other hand, interferometers are limited on large scales by their shortest baseline d_{min} which, assuming a

closed-pack configuration, is also given by $d_{\min} = D_{\text{dish}}$. Thus we will explore the capabilities of generic experiments in the $T_{\text{inst}} - D_{\text{dish}}$ plane, and in the case of interferometers we will assume a flat baseline distribution **TODO:** cite:

$$N_d(d) = \begin{cases} \frac{N_{\text{dish}}(N_{\text{dish}}-1)}{2\pi(d_{\max}^2 - D_{\text{dish}}^2)} & \text{if } D_{\text{dish}} < d \leq d_{\max}, \\ 0 & \text{otherwise} \end{cases} \quad (8)$$

TODO: Discuss foregrounds.

D. Forecasting formalism

Our formalism will distinguish between two types of tracers of the density field:

- Spectroscopic: tracers whose redshift distribution is well known. This would correspond to tracers with good radial resolution such as a narrow redshift bin of spectroscopic sources or an intensity map in a narrow frequency band, as well as other tracers with a well-known window function, such as a CMB lensing map.

- Photometric: tracers whose redshift distribution is unknown or uncertain. This would correspond to e.g. a photometric-redshift bin, a radio continuum survey or a map of the Cosmic Infrared Background.

Let us start by considering a set of sky maps corresponding to a number of tracers, and let a be the corresponding vector of maps expressed in a given basis. In the following sections we will often be in a situation where a are stored in terms of spherical harmonic coefficients and takes the form $\mathsf{a}_{\ell m} = (p_{\ell m}, s_{\ell m}^1, ... s_{\ell m}^{N_s})$, where $p_{\ell m}$ is a photometric tracer and $s_{\ell m}^i$ is a set of spectroscopic tracers. For the moment, however, we will keep the discussion general.

Assuming that a is Gaussianly distributed with zero mean and covariance $\hat{\mathsf{C}} \equiv \langle \mathsf{a}\mathsf{a}^\dagger \rangle$, its log-likelihood is given by:

$$\mathcal{L} \equiv -2\log p(\mathsf{a}) = \mathsf{a}^\dagger \hat{\mathsf{C}}^{-1} \mathsf{a} + \log(\det(2\pi\hat{\mathsf{C}})). \quad (9)$$

Now let q_i be a set of parameters modelling $\hat{\mathsf{C}}$, including (but not limited to) the parameters describing the photometric redshift distribution. A maximum-likelihood estimator for q_i can be defined by using an iterative Newton-Raphson method to minimize Eq. 9. This is described in [? ? ?], and yields the iterative algorithm:

$$q_i^n = q_i^{n-1} + [\hat{\mathsf{F}}^{-1}]_{ij} \left[\mathsf{a}^\dagger \hat{\mathsf{C}}^{-1} \hat{\mathsf{C}}_{,j} \hat{\mathsf{C}}^{-1} \mathsf{a} - \text{Tr}(\hat{\mathsf{C}}_{,j} \hat{\mathsf{C}}^{-1}) \right], \quad (10)$$

$$\hat{\mathsf{F}}_{ij} \equiv \left\langle \frac{\partial^2 \mathcal{L}}{\partial q_i \partial q_j} \right\rangle = \text{Tr}\left(\hat{\mathsf{C}}^{-1} \hat{\mathsf{C}}_{,i} \hat{\mathsf{C}}^{-1} \hat{\mathsf{C}}_{,j} \right),$$

where, in Eq. 10 there is an implicit summation over j, the sub-index $_{,i}$ implies differentiation with respect to q_i, $\hat{\mathsf{F}}$ is the Fisher matrix, q_i^n is the $n-$th iteration of the solution for q_i and the previous iteration q_i^{n-1} is used to compute $\hat{\mathsf{C}}$ and $\hat{\mathsf{C}}_{,i}$ in the second term. Note that we have simplified a pure Newton-Raphson iteration by taking the ensemble average of the likelihood Hessian (i.e. the Fisher matrix). Furthermore, in the case where the likelihood is well-approximated by a Gaussian, $\hat{\mathsf{F}}^{-1}$ is the covariance matrix of the q_i. Eq. 10 is the basis of the method proposed in [?] (with a number of simplifications) and used in [?] to constrain the redshift distribution of galaxies in the KiDS survey.

In our case, we mainly care about the uncertainty in the redshift distribution parameters included in the q_i, and therefore we will simply estimate the Fisher matrix $\hat{\mathsf{F}}$. In the case where a is a set of spherical harmonic coefficients with power spectrum $\langle \mathsf{a}_{\ell m} \mathsf{a}_{\ell'm'}^\dagger \rangle = \delta_{\ell\ell'} \delta_{mm'} \hat{\mathsf{C}}_\ell$, $\hat{\mathsf{F}}$ is given by

$$\hat{\mathsf{F}}_{ij} = \sum_{\ell=2}^{\ell_{\max}} f_{\text{sky}}(\ell + 1/2) \, \text{Tr}\left(\hat{\mathsf{C}}_\ell^{-1} \hat{\mathsf{C}}_{\ell,i} \hat{\mathsf{C}}_\ell^{-1} \hat{\mathsf{C}}_{\ell,j} \right), \quad (11)$$

where we have approximated the effects of a partial sky coverage by scaling the number of independent modes per ℓ by the sky fraction f_{sky}. The form of the power spectra $\hat{\mathsf{C}}_\ell$ for the different tracers considered in this work is given in Appendix B.

As explicitly shown in Eq. 11, smaller-scale modes carry a higher statistical weight (proportional to $\sim \ell$), and would in principle dominate the redshift distribution constraints. The smallest scales are, however, dominated by theoretical uncertainties from non-linearities in the evolution of the density field and the galaxy-halo connection, and therefore a multipole cutoff $\ell_{\max}$ must be used to contain the constraining power of systematics-dominated modes. In this paper we use a redshift-dependent cutoff defined as follows. Let z be the mean redshift of a given redshift bin, and let $\sigma^2(k_*)$ be the variance of the linear density field at that redshift on modes with wavenumber $k < k_*$:

$$\sigma^2(k_{\max}) \equiv \frac{1}{2\pi^2} \int_0^{k_*} dk \, k^2 \, P_m(k, z). \quad (12)$$

We then define the cutoff scale as $\ell_{\max}(z) = \chi(z) k_{\max}(z)$, where $k_{\max}(z)$ satisfies $\sigma(k_{\max}, z) = \sigma_{\text{thr}}$ for some choice of σ_{thr}. In what follows we will use a fiducial threshold $\sigma_{\text{thr}} = 0.75$, corresponding to $k_{\max}(z = 0) \simeq 0.2 \, h \, \text{Mpc}^{-1}$, and we will study the dependence of our results on this choice. Besides this choice of $\ell_{\max}$, we will also impose a hard cutoff for all galaxy-survey and intensity-mapping tracers of $\ell < 2000$ (thus, in reality, $\ell_{\max} = \min(\chi k_{\max}, 2000)$).

III. RESULTS

In order to forecast for the ability of future experiments to constrain photometric redshift distributions, in the following sections we will use the formalism described in Section II D with a data vector given by $a_{\ell m} = (p_{\ell m}, s^1_{\ell m}, ..., s^{N_s}_{\ell m})$, where p is a photometric redshift bin and s^i are a set of overlapping redshift bins for a spectroscopic tracer (either an intensity mapping experiment or a spectroscopic galaxy survey). The number N_s, width and redshift range of the spectroscopic redshift bins is chosen in order to adequatly sample the changes in the photometric redshift distribution. We choose the redshift bin width to be 33% of the photo-z uncertainty σ_z, which governs the variability of the redshift distribution (i.e. each redshift interval of σ_z is sampled in 3 points). In order to sample the tails of the distribution we then define the redshift range of the set of spectroscopic bins as $[z^i_b - 3\sigma_z, z^f_b + 3\sigma_z]$, where z^i_b and z^f_b are the edges of the photometric redshift bin. The number of spectroscopic redshift bins N_s is then defined in terms of these numbers.

The model parameters q_i in the following sections will be given by:

- All of the parameters needed to determine the redshift distribution (σ_z, Δz, γ_L or the amplitude $N(z)$ in different spectroscopic bins, depending on the case).

- Two overall clustering bias parameters, b_p and b_s, corresponding to the bias of the photometric and spectroscopic tracers.

- We will also include Ω_M in q_i, in order to account for the possible cosmology dependence of the results.

We will change this setup in Section III E, where we will explore the impact of the achieved constraints on the photo-z parameters on the final cosmological constraints achievable by LSST. In this section a will correspond to the 15 photometric redshift bins for LSST, for both galaxy clustering and weak lensing (i.e. 30 sets of spherical harmonics). Likewise q_i will contain the cosmological parameters $(\omega_c, \omega_b, h, w_0, w_a, A_s, n_s, \tau_{reio})$ as well as all the baseline photo-z parameters (Δz and σ_z for all redshift bins), with priors corresponding to the constraints found in the preceding sections.

A. Baseline forecasts

- First run: see Fig. 3

TODO:

- Describe results for SKA and HIRAX in comparison with DESI, Euclid, WFIRST.

- Show forecasts on parameters before and after calibration.

B. Dependence on experimental parameters

TODO:

- Show results as a function of f_{sky}, and noise level.

- Show results as a function of dish size for single-dish experiments

- Show results as a function of minimum baseline for interferometers

C. Foregrounds

TODO:

- Show results in the presence of foreground residuals.

- As a function of residual amplitude?

- Discuss correlated extragalactic foregrounds?

D. Generalized redshift distributions
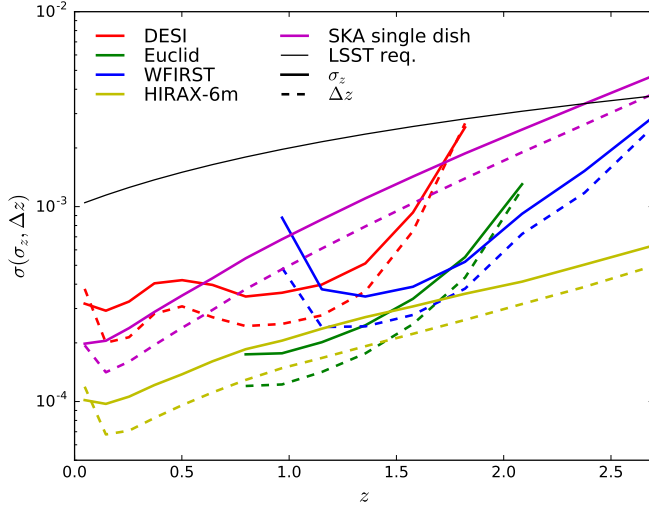
TODO:

- Include hard-tail parameters (e.g. Cauchy contribution - Voigt profile).

- Non-parametric calibration. Show results for bins of dN/dz of fixed width as a function of experiment and redshift.

E. Impact on cosmological constraints

TODO: Show effect of achieved photo-z priors on final cosmological parameters

IV. DISCUSSION

TODO: Etiam euismod. Fusce facilisis lacinia dui. Suspendisse potenti. In mi erat, cursus id, nonummy sed, ullamcorper eget, sapien. Praesent pretium, magna in eleifend egestas, pede pede pretium lorem, quis consectetuer tortor sapien facilisis magna. Mauris quis magna varius nulla scelerisque imperdiet. Aliquam non quam. Aliquam porttitor quam a lacus. Praesent vel arcu ut tortor cursus volutpat. In vitae pede quis diam bibendum placerat. Fusce elementum convallis neque. Sed dolor orci, scelerisque ac, dapibus nec, ultricies ut, mi. Duis nec dui quis leo sagittis commodo.

FIG. 3: **TODO:**

APPENDIX A: INDIVIDUAL CLUSTERING REDSHIFTS

TODO: Possibly describe formalism to sharpen redshifts for individual redshifts.

APPENDIX B: ANGULAR POWER SPECTRA

TODO: Describe models used for the angular power spectra

APPENDIX C: NOISE POWER SPECTRUM FOR INTENSITY MAPPING EXPERIMENTS

TODO: Power spectrum models used here

APPENDIX D: VOIGT PROFILE

A Voigt profile is given by a convolution of a Gaussian and a Cauchy or Lorentzian distribution, and is thus parametrized by the half-width at half-maximum of both component (γ_G and γ_L respectively here):

$$p_V(x;\gamma_G,\gamma_L) \equiv \int_{-\infty}^{\infty} dx' p_G(x';\gamma_G) \, p_L(x-x';\gamma_L), \tag{D1}$$

$$p_G(x;\gamma_G) \equiv \sqrt{\frac{\ln 2}{\pi\gamma_G^2}} \exp\left[-\ln(2)x^2/\gamma_G^2\right], \quad p_L(x;\gamma_L) \equiv \frac{\gamma_L}{\pi}\frac{1}{\gamma_L^2+x^2}. \tag{D2}$$

In order to avoid the computational complexity of evaluating Eq. D1, we will use an approximate pseudo-Voigt profile:

$$\tilde{p}_V(x;\gamma_G,\gamma_L) = \eta p_L(x;\bar{\gamma}) + (1-\eta)\,p_G(x;\bar{\gamma}), \tag{D3}$$

with expressions for η and $\bar{\gamma}$ in terms of γ_G and γ_L given by [?]:

$$\bar{\gamma}(\gamma_G,\gamma_L) = \left[\gamma_G^5 + 2.69269\gamma_G^4\gamma_L + 2.42843\gamma_G^3\gamma_L^2 + 4.47163\gamma_G^2\gamma_L^3 + 0.07842\gamma_G\gamma_L^4 + \gamma_L^5\right]^{1/5}, \tag{D4}$$

$$\eta(\gamma_G,\gamma_L) = 1.36603\frac{\gamma_L}{\bar{\gamma}} - 0.47719\left(\frac{\gamma_L}{\bar{\gamma}}\right)^2 + 0.11116\left(\frac{\gamma_L}{\bar{\gamma}}\right)^3 \tag{D5}$$

The cumulative distribution entering the redshift distribution is:

$$\int_{z_b^i}^{z_b^f} dz_{\mathrm{ph}} p(z_{\mathrm{ph}}|z, \sigma_z, \gamma_L) = \frac{\eta}{\pi} \left[\arctan\left(\frac{z_b^f - z}{\bar{\gamma}} \right) - \arctan\left(\frac{z_b^i - z}{\bar{\gamma}} \right) \right]$$

$$\frac{1-\eta}{2} \left[\mathrm{erf}\left(\frac{(z_b^f - z)\sqrt{\ln 2}}{\bar{\gamma}} \right) - \mathrm{erf}\left(\frac{(z_b^i - z)\sqrt{\ln 2}}{\bar{\gamma}} \right) \right] \tag{D6}$$

[1] η is defined as the ratio of the effective to real antenna area.